CO_2 hydrogenation to methanol over zeolite-encaged mononuclear copper centers

Yuchao Chai,[1*] Bin Qin,[1*] Bonan Li,[3] Weili Dai,[1] Guangjun Wu, [1] Naijia Guan, [1] Landong Li[1,2†]

[1] School of Materials Science and Engineering, Nankai University, Tianjin 300350, P.R. China

[2] Key Laboratory of Advanced Energy Materials Chemistry of Ministry of Education, College of Chemistry, Nankai University, Tianjin 300071, P.R. China

[3] CAS Key Laboratory of Science and Technology on Applied Catalysis, Dalian Institute of Chemical Physics, Chinese Academy of Sciences, Dalian 116023, P.R. China

*These authors contributed equally to this work.

†Corresponding author. Email: lild@nankai.edu.cn (L. L.)

Summary: The selective hydrogenation of CO_2 to methanol by renewable hydrogen source represents an attractive route for CO_2 recycling and carbon neutral. Stable catalysts with high activity and methanol selectivity are being hotly pursued, and current debates on the active site and reaction pathway need to be clarified. Here, we report the design of faujasite-encaged mononuclear Cu centers, namely Cu@FAU, for this challenging reaction. Stable methanol space-time-yield (STY) of 12.8 mmol/g_{cat}/h and methanol selectivity of 89.5 % are simultaneously achieved at a relatively low reaction temperature of 513 K, making Cu@FAU a potential methanol synthesis catalyst from CO_2 hydrogenation. With zeolite-encaged mononuclear Cu centers as the destined active sites, the unique reaction pathway of stepwise CO_2 hydrogenation over Cu@FAU is illustrated. This work provides an elegant example of catalytic reaction with explicit structure-activity relationship and highlights the power of zeolite catalysis in complex chemical transformations.

KEYWORDS: *CO_2 hydrogenation, zeolite, methanol, catalysis, mononuclear copper*

Introduction

The increasing amount of atmospheric CO_2 from anthropogenic emission is becoming a serious concern worldwide, as it can cause serious environmental problems like global warming and increased ocean acidity. Among all technically feasible approaches for reducing and recycling CO_2, the hydrogenation of CO_2 to green methanol (CH_3OH) using preferentially renewable hydrogen source has drawn great attention (*1-5*). The target product CH_3OH can be directly applied in internal combustion engines and fuel cells or be reserved as a versatile chemical feedstock (*6-8*). The CO_2-to-CH_3OH transformation is challenging due to the relative chemical inertness of CO_2 and the difficulty in controlling side reactions to obtain the single product CH_3OH. Many catalyst systems have been explored for CO_2 selective hydrogenation, including Cu-based catalysts (*9-13*), noble metal catalysts (*14,15*) and metal oxide catalysts (*16,17*), etc. (*18-20*) Thereinto, Cu-based catalysts with unparalleled advantages of low-cost and high-abundance have been intensively investigated in the past decades. $Cu/ZnO/Al_2O_3$ is currently recognized as a benchmark catalyst for CH_3OH synthesis from the hydrogenation of CO_2, CO or CO/CO_2 mixture. The inherent instability and complexity of Cu component as well as the further modifications by promoters like ZnO bring about significant debates on the active Cu sites (*21-25*) and the reaction pathway thereof (*4,26*). Cu-based catalysts with diverse Cu sites generally suffer from low CH_3OH selectivity owing to the exacerbated reverse water gas shift (RWGS) reaction to produce CO and the excessive hydrogenation to methane (CH_4) (*27,28*). In practical recycled reactor for CO_2 hydrogenation, elevated temperatures are employed to obtain reasonable CO_2 conversion and CH_3OH STY, resulting in high energy consumption and further decline in CH_3OH selectivity. On the other hand, the reaction of CO_2-to-CH_3OH is limited by thermodynamic equilibrium, and low temperatures are beneficial to attain both high equilibrium CO_2 conversion and high CH_3OH selectivity. The design of highly active Cu-based catalysts for CO_2 selective

hydrogenation to CH_3OH at low reaction temperatures is therefore possible and urgently demanded.

Zeolites are widely employed industrial catalysts and support materials with unique confinement effect (*29,30*) and ionic environment (*31*). Transition metal ions (TMIs) can be accommodated within zeolite matrix, balancing the negative charges of $[AlO_4]^-$ units, to create more functionalities (*32-35*). Isolated TMIs can be efficiently stabilized by zeolite matrix (*36,37*), providing an opportunity to construct TMIs-containing zeolites toward selective catalysis. Herein, we demonstrate the design of uniform Cu ions confined in faujasite, namely Cu@FAU, for the selective hydrogenation of CO_2 to CH_3OH. Cu@FAU catalyst with mononuclear Cu centers exhibits high CH_3OH selectivity and STY as well as perfect stability in CO_2 reduction at relatively low reaction temperatures, fulfilling the basic requirements for industrial applications. With well-defined structure of Cu@FAU model catalyst, the current debates on active Cu sites can be addressed and a clear roadmap of stepwise CO_2 reduction to CH_3OH is illustrated.

Results and Discussion

In situ hydrothermal route was developed to encapsulate Cu complexes in the matrix of faujasite (See **Supplementary Information** for details) and Cu ions confined in faujasite could be obtained *via* the calcination removal of organic ligands. Post-synthesis modulation was performed and the exchangeable Cu ions were selectively removed through repeated ion exchange with $NaNO_3$ aqueous solution, leaving stable and unexchangable Cu ions confined in faujasite. X-ray diffraction (XRD) pattern identifies the typical FAU topology in pure-phase (**Figure S1**) and Ar sorption isotherms reveal the uniform microporous structure (**Figure S2**) of Cu@FAU. Microscopy analyses indicate the characteristic octahedral faujasite morphology with crystal size of 1-2 μm and the ultra-dispersion of Cu species with loading of ~4.5 wt%. (**Figure S3** and **S4**).

A single $Cu^{2+}\rightarrow Cu^{+}$ reduction peak centered at ~443 K was observed for Cu@FAU (**Figure S5**), while complex $Cu^{+}\rightarrow Cu^{0}$ reduction peaks in the temperature region of

523-873 K were observed for Cu-FAU and Cu/FAU samples (*38,39*). That is, uniform Cu ions were formed and efficiently stabilized by zeolite matrix in Cu@FAU, in great contrast to the cases of Cu-FAU and Cu/FAU where significant amounts of CuOx species were present as observed in the TEM images (**Figure S6**). The valance state of +2 in Cu@FAU was confirmed by Cu K-edge X-ray absorption near-edge structure (XANES) spectrum (**Figure 1a**) and a prominent peak at ~2.0 Å due to the first shell of Cu-O path with average coordination number of 3.8 was obtained in the Fourier-transformed (FT) k^2-weighted extended X-ray absorption fine structure (EXAFS) spectrum (**Figure 1b**, **Figure S7** and **Table S1**) and the wavelet-transformed (WT) EXAFS oscillations (**Figure 1c**). The fine structure of Cu@FAU and the exact location of Cu sites in faujasite were identified by synchrotron XRD (**Figure S8**). According to the results from Rietveld refinement, the Cu sites exclusively situated in the center of six-membered ring, shared by the sodalite cage and supercage of zeolite (**Figure 1d**). The possible structure of Cu^{2+} in faujasite was also screened by density functional theory (DFT) calculations and the configuration of Cu^{2+} sitting in the six-membered ring containing Al pairs in the *para-* or *meta-* positions could be optimized (**Figure S9**). The local coordination environment of Cu sites in faujasite from DFT calculations is shown in **Figure 1e**, and the bonding parameters are in good consistency with those from synchrotron X-ray absorbance spectroscopy (**Table S1**). These results demonstrate the successful construction of Cu@FAU containing uniform and well-defined mononuclear Cu sites, which is analogous to a typical coordination compound with Cu^{2+} as the central ion and faujasite framework as the ligand.

Figure 2a shows the results of CO_2 hydrogenation over representative Cu-based catalysts under relatively mild reaction conditions, *i.e.*, at 513 K and in the feed gas of 3.0 MPa CO_2-H_2 (H_2/CO_2 = 3:1). All Cu-containing zeolites, namely Cu-FAU, Cu/FAU and Cu@FAU, can catalyze the CO_2-to-CH_3OH transformation, with CO and methane as major byproducts from RWGS and methanation reactions (**Figure S10**), respectively. Cu@FAU is the most active catalyst with ~12% CO_2 conversion and ~90% CH_3OH selectivity, offering a CH_3OH STY of 12.8 mmol/g_{cat}/h distinctly higher than that of Cu-FAU (4.7 mmol/g_{cat}/h) and Cu/FAU (6.7 mmol/g_{cat}/h). The catalytic performance of

Cu-containing zeolites seems to be controlled by specific Cu sites and their chemical environment. Notably, similar CO_2 conversion was achieved with Cu@FAU (4.5wt% Cu) and commercial $Cu/ZnO/Al_2O_3$ (63.0wt% Cu) catalysts despite the huge difference in Cu loading. Cu@FAU exhibits significantly higher CH_3OH selectivity than $Cu/ZnO/Al_2O_3$ at 473-553 K with comparable CO_2 conversions (**Figure S11**). Cu@FAU surpasses commercial $Cu/ZnO/Al_2O_3$ catalyst in CO_2 selective hydrogenation at low reaction temperatures.

The temperature-dependent behaviors of Cu@FAU catalyst in CO_2 hydrogenation are shown in **Figure 2b**. The CO_2 conversion increases almost linearly with increasing reaction temperature from 453 to 573 K, and meanwhile two-stage declines in CH_3OH selectivity are observed, namely the milder declines from 453 to 513 K and the severer declines from 513 to 573 K. The reaction temperature of 513 K can be optimized in view of both CO_2 conversion and CH_3OH selectivity. Higher pressure and gas hourly space velocity (GHSV) are beneficial to the methanol selectivity (**Figure S12, Figure S13**), and CH_3OH selectivity can be promoted to 92.5 % with optimized reaction parameters. The catalytic performance of Cu@FAU, in terms of CH_3OH selectivity and STY, is superior to all known Cu-based catalysts under comparable reaction conditions (**Figure 2c**, **Table S2**), and more importantly, the remarkable catalytic performance is achieved with Cu as a single active component free of modifiers. Cu@FAU catalyst demonstrates good stability and no activity loss or selectivity decline can be observed for over 200 h run of CO_2 hydrogenation (**Figure 2d**, carbon balance >95%), in significant contrast to Cu-FAU (**Figure S14**) and Cu/FAU (**Figure S15**). Stability is a fatal issue for CH_3OH synthesis from CO and/or CO_2 hydrogenation, and Cu-based catalysts generally suffer from fast deactivation due to metal sintering. For Cu@FAU catalyst, the isolated Cu ions are efficiently stabilized by zeolite matrix and their coordination environment can be well preserved in long-term running, as confirmed by EXFAS analyses (**Table S1**, **Figure S16**). Overall, Cu@FAU appears to be a qualified catalyst for CH_3OH production from CO_2 hydrogenation at low reaction temperatures, offering high CH_3OH and STY as well as perfect stability.

CO_2 hydrogenation generally requires both CO_2 and H_2 activation, followed by the stabilization of reaction intermediates for controllable hydrogenation. Dihydrogen cannot be activated on Cu@FAU at the reaction temperature of 513 K, as indicated by the absence of HD signal (m/z= 3) in H_2-D_2 stream (**Figure 4a**) (*40*). Upon the introduction of CO_2 pulses, the signals of H_2 and D_2 decline while the HD signal appears, accompanied by the formation of CH_3OH and deuterated CH_3OH (control experiment shown in **Figure S17**, **Figure S18**). These observations clearly demonstrate the CO_2-assisted dihydrogen activation on Cu@FAU and the subsequent hydrogenation of CO_2 to CH_3OH. The surface species involved in the hydrogenation process were then monitored by *in situ* diffuse reflectance infrared Fourier transform spectroscopy (DRIFTS). A series of organic surface species were observed and most of these species reached dynamic equilibrium at the early stage of reaction (**Figure 3b**). Typically, the infrared band at 1250 cm^{-1} is assigned to the C-O asymmetric stretching vibrations of mono- or bidentate HCOO* species, and the band at 1335 cm^{-1} assigned to the C-O asymmetric stretching vibrations of HCOOH* species with contribution from bending vibrations. The band at 1385 cm^{-1} is due to the bending vibrations of CH_3O* species and the paired bands at 1465 and 1495 cm^{-1} due to the bending vibrations of CH_3OH* species. The band at 1385 cm^{-1} is related to the C-O asymmetric stretching vibrations of CH_2O* with adjacent co-adsorbed H_2O and the contribution from C-H bending vibrations. The band at 2915 cm^{-1} is explicitly related to the C-H stretching vibrations of H_2COOH* species (*17,19,41,42*). DFT calculations were employed to support the above assignments, and the structure of key organic species and their vibration frequencies are summarized in **Figure 3c** and **Table S3**. In deuterium labeling experiments, the C-D stretching vibrations of DCOO* (2160 cm^{-1}), DCOOD* (2095 cm^{-1}) and CD_3O* (2060 cm^{-1}) species were observed (**Figure 3d**) (*17,43*). All these observations hint to the stepwise CO_2 reduction by dihydrogen on the Cu@FAU, which appears to be quite different to the conventional CO pathway (*24*). Accordingly, Cu@FAU catalyst shows very low activity in the hydrogenation of CO, with ~2.5% CO conversion at 513 K (**Figure S19**).

DFT calculations were finally employed to clarify the reaction pathway of CO_2

hydrogenation to CH_3OH over Cu@FAU, with mononuclear Cu centers confined in faujasite as the catalytically active sites. In the first step, gaseous CO_2 adsorbs on Cu site in a linear configuration (ln-CO_2*) with adsorption energy of −0.22 eV at 0 K, followed by the adsorption of dihydrogen. The dihydrogen undergoes facile dissociation into a hydride bonded to Cu site and a proton bonded to adjacent O site *via* **TS1** (E_a = 0.75 eV, E_r = 0.32 eV). Clearly, the dihydrogen is activated by classical Lewis pairs (Cu-O) with the assistance from adsorbed CO_2 species, as confirmed by the pulse-response experiment results in **Figure 3a**. The hydride transfer to the C atom of the ln-CO_2* results in the formation of the monodentate formate (mono-HCOO*) *via* **TS2** (E_a = 0.64 eV, E_r = -0.12 eV). The mono-HCOO* rapidly transforms to the bidentate formate (bi-HCOO*, E_r = -0.29 eV), which is further protonated to the HCOOH* *via* **TS3** (E_a = 0.37 eV, E_r = 0.17 eV). The second dihydrogen molecule then dissociates into a hydride and a proton at the Cu-O pair site and the HCOOH* is hydrogenated to the H_2COOH* *via* **TS4** (E_a = 0.65 eV, E_r = 0.09 eV). Through a simple rotation, the H_2COOH* reacts with the proton to form the CH_2O* and the H_2O* *via* **TS5** (E_a = 0.00 eV, E_r = -0.29 eV). The H_2O* leaves the active site with the desorption energy of 0.39 eV and enables the third dihydrogen dissociation at the Cu-O pair site. The formed CH_2O* is hydrogenated to the CH_3O* *via* **TS6** (E_a = 0.63 eV, E_r = -0.64 eV) and the CH_3OH* is formed by the protonation of the CH_3O* *via* **TS7** (E_a = 0.00 eV, E_r = -0.58 eV). Finally, the CH_3OH* desorbs from the active site (E_r = 0.84 eV) and the catalytic cycle ends, and the Cu@FAU catalyst does not promote further reactions of CH_3OH at 513 K, which was consistent with the CH_3OH-feeding experiment shown in **Figure S20**. For a direct view, the complete reaction pathway of CO_2 hydrogenation to CH_3OH over Cu@FAU model catalyst and the calculated Gibbs free energy profile are shown in **Figure 4** (adsorption energy of key intermediates listed in **Table S4, Table S5**). Some of the key reaction intermediates like HCOOH*, H_2COOH*, CH_3O* and CH_3OH* have been successfully captured by *in situ* DRIFTS, as shown in **Figure 3d**.

According to above analyses, all the energy barriers from **TS1** to **TS7** are less than 0.75 eV and the reaction energies are less than 0.32 eV, indicating that CH_3OH production from CO_2 hydrogenation on zeolite confined mononuclear Cu centers is

thermodynamically and kinetically favorable. The first CO_2-assisted dihydrogen dissociation has the highest activation barrier, and it should be the rate-determining step for the overall reaction. At the optimized temperature of 513 K, the energy barriers and reaction energies are reasonable (**Figure S21**). The high catalytic activity of the Cu@FAU originates from the unique configuration of Cu^{2+} sitting in the six-membered ring, containing classical Lewis pairs of Cu-O units. The C-containing intermediates can effectively adsorb on Cu sites and assist the dihydrogen activation on Cu-O pairs for subsequent hydrogenation. We also search for the bent configuration of CO_2 (bt-CO_2*) by structure optimization, which is found to be extremely unstable and undergoes spontaneously transformation to ln-CO_2* on Cu site. Thereupon, the traditional protonation of bt-CO_2* to COOH* followed by dissociation to CO* (*26,44*) or bt-CO_2* direct dissociation to CO* (*45*) will not occur on Cu@FAU.

Conclusion

The selective hydrogenation of CO_2 to CH_3OH provides a technically feasible route for CO_2 recycling and carbon neutral. The reaction process is very complex and requires the well-balanced C-O dissociation and dihydrogen activation. A complicated catalyst system of Cu/ZnO/Al_2O_3 is currently employed to achieve high activity and moderate selectivity to CH_3OH as well as good catalyst stability, which also brings about significant debates on the active site and reaction mechanism. Herein, we demonstrate that zeolite-encaged mononuclear Cu centers, namely Cu@FAU, can efficiently catalyze the stable CO_2-to-CH_3OH transformation at relatively low reaction temperature of 513 K, offering a high CH_3OH STY of 12.8 mmol/g_{cat}/h at selectivity of ~90 %. The reaction sequence of CO_2 hydrogenation over well-defined Cu@FAU catalyst and the full catalytic cycle are successfully determined. It is disclosed that all the reaction steps can take place on Cu sites and the adjacent framework O atoms play indispensable roles by constructing Cu-O pairs to induce dihydrogen activation. The unique zeolite catalyst system and reaction pathway contribute to the success of CO_2-to-CH_3OH process for carbon neutral, and may trigger some new thoughts for other complex chemical transformations.

Experimental Procedures

Chemical reagents

Copper nitrate [$Cu(NO_3)_2$, Aladdin], sodium aluminate ($NaAlO_2$, Aladdin), 3-[2-(2-aminoethylamino)ethylamino]propyl-trimethoxysilane (TAPTS, Macklin, CAS: 35141-30-1), sodium hydroxide (NaOH, Aladdin), silica sol (50 wt.% SiO_2, Alfa Aesar), sodium nitrate ($NaNO_3$, Aladdin). All chemical reagents are of analytical grade and used directly without further purification.

Hydrothermal synthesis of Cu@FAU

Cu@FAU was synthesized *via* a ligand-protected *in situ* hydrothermal route. In a typical experiment, 4.13 g $Cu(NO_3)_2$ was added into 98 mL deionized water containing 11.71 g TAPTS and stirred for 30 minutes to obtain the Cu-TAPTS solution. Then, 5.80 g $NaAlO_2$ and 6.05 g NaOH were added into the solution in turn. After stirring for 1 h, 34 g silica sol (50 wt.% SiO_2) was dropwise added into the above mixture under vigorous stirring to form the synthesis gel. Finally, the gel with the molar ratio of 7.8 SiO_2: 1 Al_2O_3: 2.2 Na_2O: 0.6 Cu-TAPTS: 174 H_2O was transferred into an autoclave and heated at 373 K for 4 days under static conditions. The solid was collected by centrifuging, washed with water, dried at 353 K overnight and calcined in flowing air at 823 K for 6 h.

The calcined solid samples were subsequently ion-exchanged with 1 M $NaNO_3$ solution for three times to selectively remove the Cu ions at the exchangeable sites, dried at 353 K overnight, and calcined in flowing air at 823 K for 6 h to derive Cu@FAU sample for catalysis.

Preparation of Cu-FAU and Cu/FAU

Commercial Na-FAU zeolite (Si/Al = 3.5) was employed as zeolite host and Cu species were introduced to the zeolite by ion-exchanged with 1.0 M $Cu(NO_3)_2$ aqueous solution for three times at the constant temperature of 353 K. After each ion-exchange process, the slurry was filtered and washed with distilled water. The final solid product was dried at 353 K overnight and calcined in flowing air at 823 K for 6 h to derive Cu-FAU.

Cu species were also introduced into Na-FAU zeolite (Si/Al = 3.5) by wet impregnation, followed by similar drying and calcination steps. The final product was denoted as Cu/FAU.

Sample characterization

The chemical compositions of samples were analyzed on an IRIS Advantage inductively coupled plasma atomic emission spectrometer (ICP-AES).

The X-ray diffraction (XRD) patterns of selected zeolite samples were recorded on a Bruker D8 diffractometer using Cu-Kα radiation (λ= 0.1541 nm) in the region of 2θ = 5-50º at a scanning rate of 6 º/min. High resolution synchrotron X-ray powder diffraction data of selected samples were collected at Beamline I11 of Diamond Light Source using multi-analysing crystal-detectors and monochromated radiation [λ =0.826126(2) Å].

The surface areas of samples were determined by Ar adsorption/desorption isotherms at 87 K collected on a Quantachrome iQ-MP gas adsorption analyser. The total surface area was calculated *via* the Brunauer Emmett Teller (BET) equation and the micropore volume was determined using the t-plot method.

Transmission electron microscopy (TEM) images of selected samples were acquired on a FEI Tecnai G2 F20 electron microscope.

The experiments of temperature-programmed reduction by hydrogen (H_2-TPR) were performed on a Quantachrome ChemBET 3000 chemisorption analyzer. In a typical experiment, the sample of ~0.1 g was calcined in dry air at 823 K for 1 h and cooled to 323 K in flowing Ar. H_2-TPR profile was recorded in flowing 5%H_2/Ar at a heating rate of 10 K /min from 323 to 1123 K.

The X-ray absorption spectra (XAS) were measured at the BL11B, Shanghai Synchrotron Radiation Facility (SSRF) (*46*), including X-ray absorption near-edge structure (XANES) and extended X-ray absorption fine structure (EXAFS) spectra at the Cu K-edge. A Si (111) double-crystal monochromator was used for the energy selection. The energy was calibrated by Cu foil as a reference and all samples were measured in the transmission mode. The Athena software package was used to analyze the data.

Catalytic reaction of CO_2 hydrogenation

The catalytic reaction of CO_2 hydrogenation was carried out in a high-pressure fixed-bed continuous-flow reactor. Typically, catalyst sample of 0.2 g was placed in the quartz reactor, pretreated in Ar at 673 K for 1 h, and cooled down to designated reaction temperature. Afterwards, the reaction was conducted under the reaction conditions of 1.0-4.0 MPa, 453-573 K, $V_{H2}/V_{CO2}/V_{Ar}$ of 72/24/4, and gas hourly space velocity (GHSV) of 8000-20,000 /h. The products were analyzed using an online gas chromatograph (Shimadzu 2010SE) equipped with a thermal conductivity

detector (TCD) and a flame ionization detector (FID). A TDX-01 packed column was connected to the TCD and an RT-Q-BOND-PLOT capillary column was connected to the FID. Product selectivity was calculated on a molar carbon basis, and the TCD and FID signals were correlated by the signal of methane.

***In situ* diffuse reflectance infrared Fourier transform spectroscopy**

The reaction of CO_2 hydrogenation to methanol was *in situ* monitored by diffuse reflectance infrared Fourier transform spectroscopy (DRIFTS). The experiments were performed on a Bruker Tensor 27 spectrometer equipped with an *in situ* reaction chamber and a liquid N_2 cooled high sensitivity mercury cadmium telluride detector. Typically, ~20 mg of finely-ground catalyst powders were placed in the reaction chamber and pretreated in Ar at 673 K for 1 h. After cooling down to the designated temperature, the reactant gas mixture containing H_2/CO_2 (3/1) or D_2/CO_2 (3/1) was fed into the chamber at GHSV of 12000 h^{-1}, and time-resolved spectra were recorded at a resolution of 4 cm^{-1} and with an accumulation of 128 scans against blank background.

Computational methods and modeling

The spin-polarized DFT calculations were performed using the Vienna ab initio simulation package (VASP) (*47,48*). The Perdew-Burke-Ernzerhof (PBE) exchange-correlation functional (*49*) and the projector-augmented wave (PAW) potentials (*50*) were used to describe the electron-ion interaction. The Bayesian error estimation functional with van der Waals correlation (BEEF-vdW) (*51*) and an energy cut-off of 400 eV were employed in this study. All structures were optimized using Γ point. The electronic energy of the supercell was converged to 10-4 eV, and the force on all unconstrained atoms were converged to 0.01 eV Å.

The structure of the Cu@FAU zeolite was built according to the characterization results. All atoms in the structure were allowed to relax. The zero-point energies (ZPE), enthalpies, entropies, and Gibbs free energies were calculated from harmonic frequencies, identical to our previous work (*52*). Transition states were obtained using the climbing image nudged elastic band (CI-NEB) method (*53,54*) and confirmed by harmonic frequencies.

Acknowledgements

We thank Dr. Sihai Yang at University of Manchester for help in Rietveld refinement. **Funding:** This work is supported by the National Natural Science Foundation of China (22121005, 22002062, 22025203), the China National Postdoctoral Program for Innovative Talents (BX20200171) and the Fundamental Research Funds for the Central Universities (Nankai University). **Authors contributions:** Y.C. conducted the sample synthesis and catalytic study. B.Q. performed the theoretical calculations. B.L. collected and analysed the X-ray absorption spectroscopy data. W.D., G.W. and N.G. analyzed the data and provided helpful discussions. L.L. directed and supervised the project. Y.C., B.Q. and L.L. prepared the manuscript. **Competing interests:** The authors declare no competing interests.

Supplementary Information

Figs S1 to S20

Tables S1 to S5

Reference (*46-84*)

References

1. A. M. Appel et al., Frontiers, opportunities, and challenges in biochemical and chemical catalysis of CO_2 fixation. *Chem. Rev.* **113**, 6621–6658 (2013).

2. E. V. Kondratenko, G. Mul, J. Baltrusaitis, G. O. Larrazábal, J. Perez-Ramírez, Status and perspectives of CO_2 conversion into fuels and chemicals by catalytic, photocatalytic and electrocatalytic processes. *Energy Environ. Sci.* **6**, 3112–3135 (2013).

3. A. Goeppert, M. Czaun, J. -P. Jones, G. K. S. Prakash, G. A. Olah, Recycling of carbon dioxide to methanol and derived products-closing the loop. *Chem. Soc. Rev.* **43**, 7995–8048 (2014).

4. X. Jiang, X. W. Nie, X. W. Guo, C. S. Song, J. G. Chen, Recent advances in carbon dioxide hydrogenation to methanol via heterogeneous catalysis. *Chem. Rev.* **120**, 7984−8034 (2020).

5. S. T. Bai et al., Homogeneous and heterogeneous catalysts for hydrogenation of CO_2 to methanol under mild conditions. *Chem. Soc. Rev.* **50**, 4259–4298 (2021).

6. G. A. Olah, Beyond oil and gas: the methanol economy. *Angew. Chem. Int. Ed.* **44**, 2636–2639 (2005).

7. J. P. Holdren, Science and technology for sustainable well-being. *Science* **319**, 424–434 (2008).

8. I. Yarulina, A. D. Chowdhury, F. Meirer, B. M. Weckhuysen, J. Gascon, Recent trends and fundamental insights in the methanol-to-hydrocarbons process. *Nat. Catal.* **1**, 398–411 (2018).

9. J. Graciani et al., Highly active copper-ceria and copper-ceria-titania catalysts for methanol synthesis from CO_2. *Science* **345**, 546–550 (2014).

10. B. An et al., Confinement of ultrasmall Cu/ZnOx nanoparticles in metal-organic frameworks for selective methanol synthesis from catalytic hydrogenation of CO_2. *J. Am. Chem. Soc.* **139**, 3834–3840 (2017).

11. E. Lam et al., Isolated Zr surface sites on silica promote hydrogenation of CO_2 to CH_3OH in supported Cu catalysts. *J. Am. Chem. Soc.* **140**, 10530–10535 (2018).

12. K. Larmier et al., CO_2-to-methanol hydrogenation on zirconia-supported copper nanoparticles: Reaction intermediates and the role of the metal-support interface. *Angew. Chem. Int. Ed.* **129**, 2358–2363 (2017).

13. H. Zhou et al., Engineering the Cu/Mo_2CTx (MXene) interface to drive CO_2 hydrogenation to methanol. *Nat. Catal.* **4**, 860–871 (2021).

14. H. Bahruji et al., Pd/ZnO catalysts for direct CO_2 hydrogenation to methanol. *J. Catal.* **343**, 133–146 (2016).

15. M. Frei et al., Atomic-Scale Engineering of Indium Oxide Promotion by Palladium for Methanol Production via CO_2 Hydrogenation. *Nat. Commun.* **10**, 3377−3388 (2019).

16. O. Martin et al., Indium oxide as a superior catalyst for methanol synthesis by CO_2 hydrogenation. *Angew. Chem. Int. Ed.* **55**, 6261–6265 (2016).

17. J. Wang et al., A highly selective and stable ZnO-ZrO_2 solid solution catalyst for CO_2 hydrogenation to methanol. *Sci. Adv.*, **3**, e1701290 (2017).

18. F. Studt et al., Discovery of a Ni-Ga catalyst for carbon dioxide reduction to methanol. *Nat. Chem.* **6**, 320–324 (2014).

19. J. Hu et al., Sulfur vacancy-rich MoS_2 as a catalyst for the hydrogenation of CO_2 to methanol, *Nat. Catal.* **4**, 242–250 (2021).

20. C. Meng et al., Oxygen-deficient metal oxides supported nano-intermetallic $InNi_3C_{0.5}$ toward efficient CO_2 hydrogenation to methanol. *Sci. Adv*. **7**, eabi6012 (2021).

21. T. Lunkenbein, J. Schumann, M. Behrens, R. Schlögl, M. G. Willinger, Formation of a ZnO overlayer in industrial Cu/ZnO/Al_2O_3 catalysts induced by strong metal-support interactions. *Angew. Chem. Int. Ed.* **54**, 4544–4548 (2015).

22. S. Kuld et al., Quantifying the promotion of Cu catalysts by ZnO for methanol synthesis. *Science* **352**, 969–974 (2016).

23. A. Beck et al., Following the structure of copper-zinc-alumina across the pressure gap in carbon dioxide hydrogenation. *Nat. Catal.* **4**, 488–497 (2021).

24. M. Behrens et al., The active site of methanol synthesis over Cu/ZnO/Al_2O_3 industrial catalysts. *Science* **336**, 893–897 (2012).

25. S. Kattel, P. J. Ramírez, J. G. Chen, J. A. Rodriguez, P. Liu, Active sites for CO_2 hydrogenation to methanol on Cu/ZnO catalysts. *Science* **355**, 1296–1299 (2017).

26. S. Kattel, B. H. Yan, Y. Yang, J. G. Chen, P. Liu, Optimizing binding energies of key intermediates for CO_2 hydrogenation to methanol over oxide-supported copper, *J. Am. Chem. Soc.* **138**, 12440–12450 (2016).

27. Z. He et al., Synthesis of liquid fuel via direct hydrogenation of CO_2, *Proc. Natl. Acad. Sci.* **116** 12654-12659 (2016).

28. M. D. Porosoff, B. H. Yan, J. G. Chen, Catalytic reduction of CO_2 by H_2 for synthesis of CO, methanol and hydrocarbons: challenges and opportunities, *Energy Environ. Sci.* **9**, 62-73 (2016).

29. A. Janda, B. Vlaisavljevich, L. -C. Lin, B. Smit, A. T. Bell, Effects of zeolite structural confinement on adsorption thermodynamics and reaction kinetics for monomolecular cracking and dehydrogenation of n-butane. *J. Am. Chem. Soc.* **138**, 14, 4739–4756 (2016).

30. Y. Chai, W. Dai, G. Wu, N. Guan, L. Li, Confinement in a zeolite and zeolite catalysis. *Acc. Chem. Res.* **54**, 2894–2904 (2021).

31. N. Pfriem et al., Role of the ionic environment in enhancing the activity of reacting molecules in zeolite pores. *Science* **372**, 952–957 (2021).

32. B. E. R. Snyder, M. L. Bols, R. A. Schoonheydt, B. F. Sels, E. I. Solomon, Iron and copper active sites in zeolites and their correlation to metalloenzymes. *Chem. Rev.* **118**, 2718–2768 (2018).

33. B. E. R. Snyder et al., The active site of low-temperature methane hydroxylation in iron-containing zeolites. *Nature* **536**, 317–321 (2016).

34. V. L. Sushkevich, D. Palagin, M. Ranocchiari, J. A. V. Bokhoven, Selective anaerobic oxidation of methane enables direct synthesis of methanol. *Science* **356**, 523–527 (2017).

35. C. Paolucci et al., Dynamic multinuclear sites formed by mobilized copper ions in NOx selective catalytic reduction. *Science* **357**, 898–903 (2017).

36. Y. Chai et al., Acetylene-selective hydrogenation catalyzed by cationic nickel confined in zeolite. *J Am. Chem. Soc.* **141**, 9920–9927 (2019).

37. Y. Chai et al., Control of zeolite pore interior for chemoselective alkyne/olefin separations. *Science* **368**, 1002–1006 (2020).

38. P. D. Costa, B. Modén, G. D. Meitzner, D. K. Lee, E. Iglesia, Spectroscopic and chemical characterization of active and inactive Cu species in NO decomposition catalysts based on Cu-ZSM-5. *Phys. Chem. Chem. Phys.* **4**, 4590–4601 (2002).

39. G. Brezicki, J. D. Kammert, T. B. Gunnoe, C. Paolucci, R. J. Davis, Insights into the speciation of Cu in the Cu-H-mordenite catalyst for the oxidation of methane to methanol. *ACS Catal.* **9**, 5308−5319 (2019).

40. X. Deng et al., Homogeneous-like alkyne selective hydrogenation catalyzed by cationic nickel confined in zeolite. *CCS Chem.* **3**, 1101–1114 (2021).

41. L. Wang et al., Silica accelerates the selective hydrogenation of CO_2 to methanol on cobalt catalysts. *Nat Commun.* **11**, 1033 (2020).

42. L. Ding et al., CO_2 hydrogenation to ethanol over Cu@Na-Beta. *Chem* **6**, 1–17 (2020).

43. J. S. Huberty, R. J. Madix, An FTIR study of the bonding of methoxy on Ni(100): effects of coadsorbed sulfur, carbon monoxide and hydrogen. *Surf. Sci.* **360**, 144–156 (1996).

44. S. Dang et al., Rationally designed indium oxide catalysts for CO_2 hydrogenation to methanol with high activity and selectivity. *Sci. Adv.* **6**, eaaz2060 (2020).

45. Q. L. Tang, Q. L. Hong, Z. P. Liu, CO_2 fixation into methanol at Cu/ZrO_2 interface from first principles kinetic Monte Carlo. *J. Catal.* **263**, 114–122 (2009).

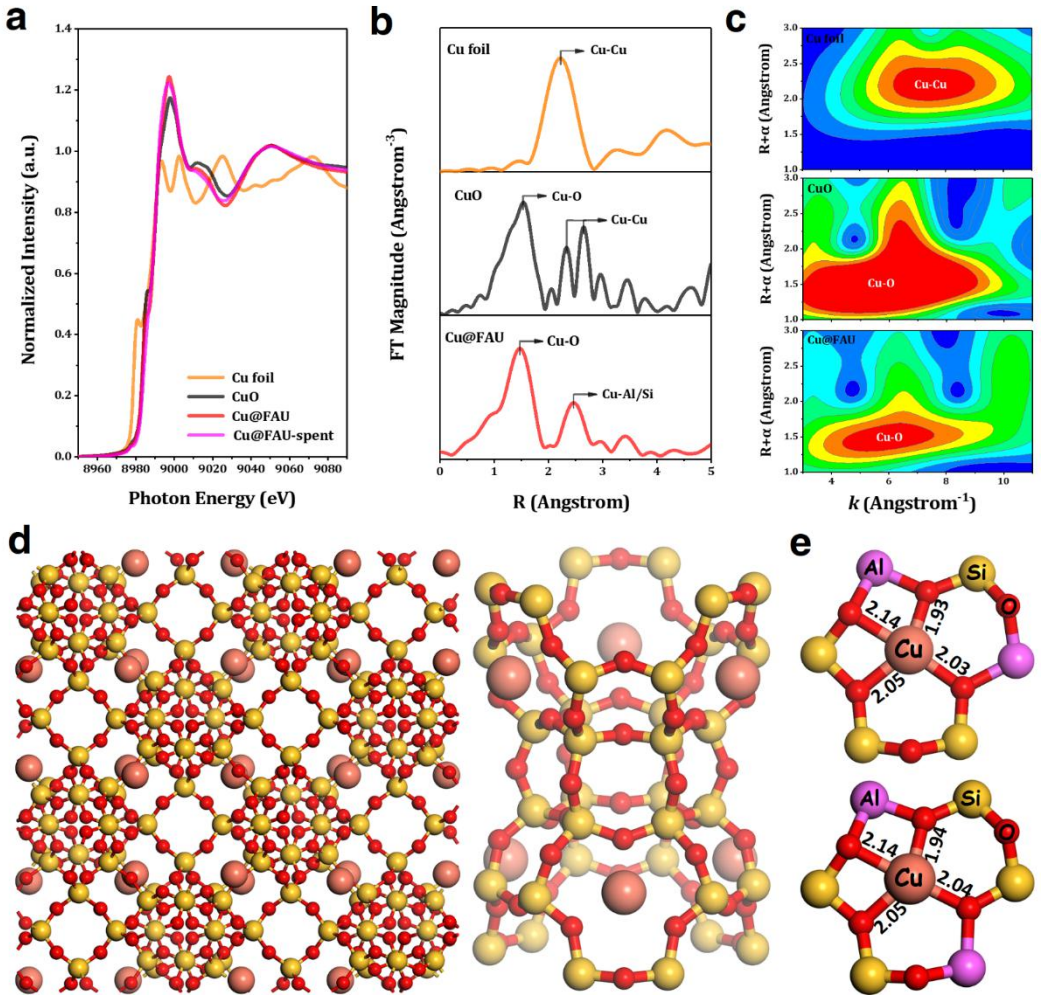

Figure 1 Fine structure of Cu@FAU model catalyst. (**a**) Cu K-edge XANES spectra of Cu foil, CuO, Cu@FAU and spent Cu@FAU; (**b**) FT k^2-weighted EXAFS spectra of Cu foil, CuO and Cu@FAU; (**c**) WT EXAFS oscillations of Cu foil, CuO and Cu@FAU; (**d**) Schematic view of Cu@FAU from synchrotron XRD Rietveld refinement; (**e**) Local coordination environment of Cu sites in faujasite from DFT calculations with bond length shown in the unit of angstrom.

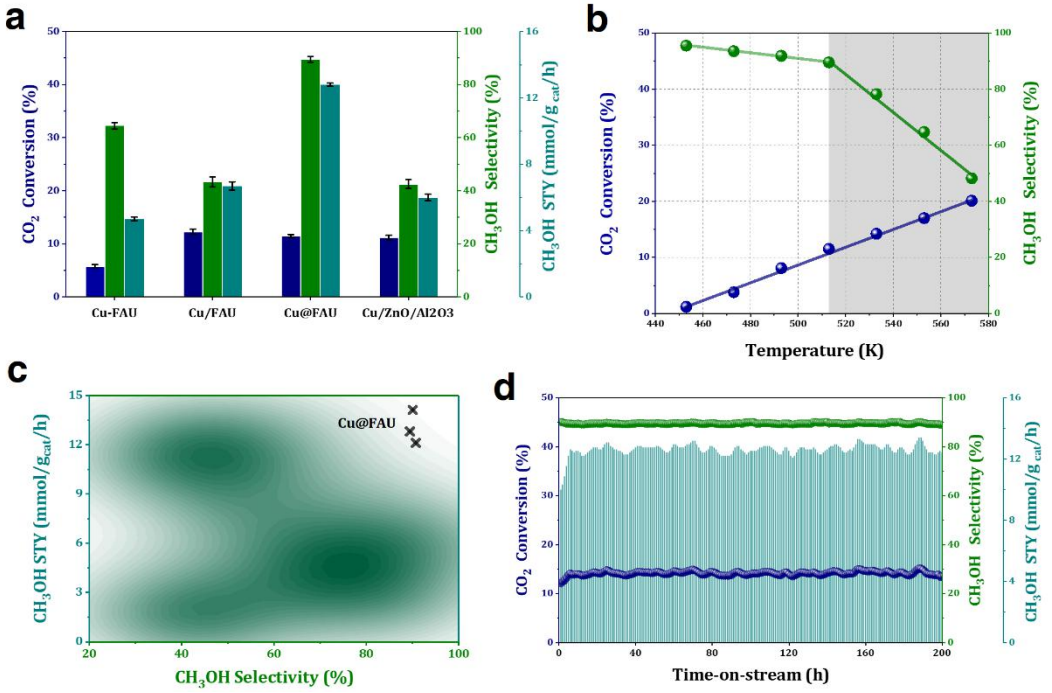

Figure 2 Catalytic performance of Cu@FAU in CO_2 selective hydrogenation. (a) Representative Cu-based catalysts in CO_2 hydrogenation. Reaction conditions: 0.15 g catalyst, H_2/CO_2= 3/1, 3 MPa, 513 K, GHSV= 12000 h^{-1}; (**b**) Temperature-dependent behaviors of Cu@FAU catalyst in CO_2 hydrogenation. Reaction conditions: 0.15 g catalyst, H_2/CO_2= 3/1, 3 MPa, GHSV= 12000 h^{-1}; (**c**) Literature survey of Cu-based catalysts for CO_2 hydrogenation. CH_3OH selectivity and STY plotted for comparison; (**d**) Stability test of Cu@FAU catalyst in CO_2 hydrogenation. Reaction conditions: 0.15 g catalyst, H_2/CO_2 = 3/1, 3MPa, 513 K, GHSV=12000 h^{-1}.

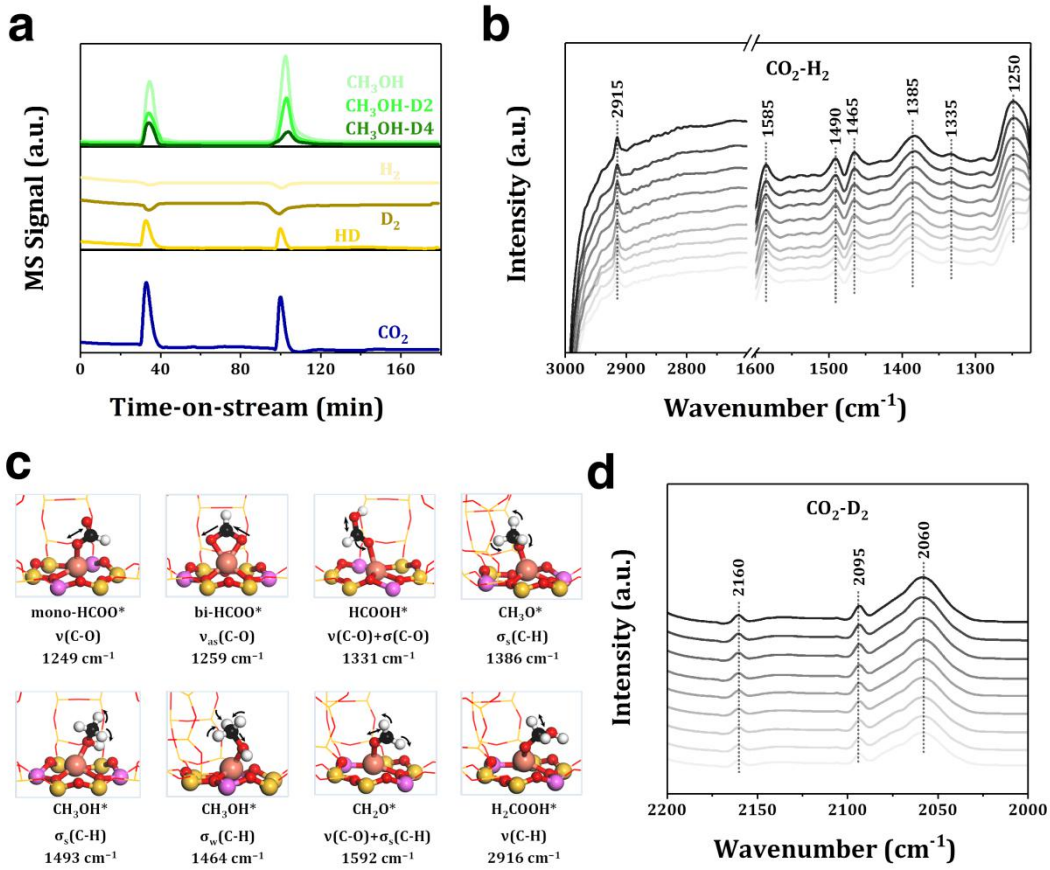

Figure 3 Characteristics of CO_2 selective hydrogenation over Cu@FAU catalyst. (**a**) Mass spectrometry responses of CO_2 pulses fed to Cu@FAU in H_2-D_2 stream. Reaction conditions: 0.2 g catalyst, 0.4 MPa, 513 K, 5 mL/min CO_2, 15 mL/min H_2-D_2 (1/1); (**b**) *In situ* DRIFT spectra of surface species formed on Cu@FAU in CO_2-H_2 stream. Time-dependent spectra recorded within 30 min, from light to dark curves. Reaction conditions: 0.02g catalyst, 3.0 MPa, 513 K, 5 mL/min CO_2, 15 mL/min H_2; (**c**) Calculated structure of key surface intermediates and their vibration frequencies; (**d**) *In situ* DRIFT spectra of surface species formed on Cu@FAU in CO_2-D_2 stream. Reaction conditions: 0.02g catalyst, 3.0 MPa, 513 K, 5 mL/min CO_2, 15 mL/min D_2.

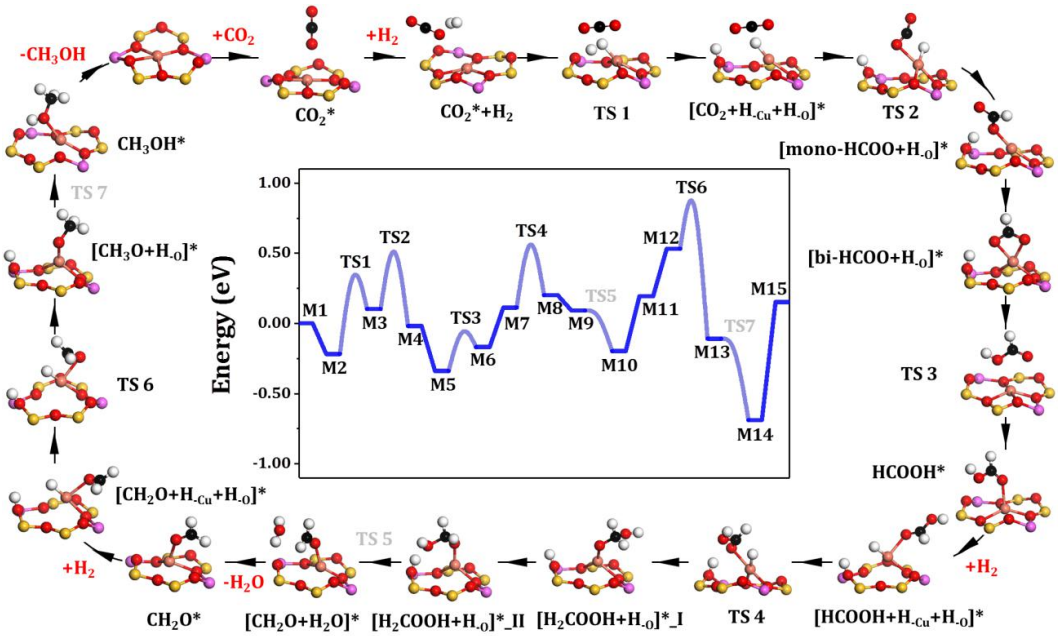

Figure 4 Reaction pathway of CO_2 hydrogenation to CH_3OH on mononuclear Cu centers. Elementary reaction steps of CO_2 hydrogenation over Cu@FAU model catalyst and calculated Gibbs free energy profile with ZPE correction at 0 K.